The Complement Regulator C4b-Binding Protein (C4BP) Interacts with both the C4c and C4dg Subfragments of the Parent C4b Ligand: Evidence for Synergy in C4BP Subsite Binding†

Elisa Leung,‡ Anna M. Blom,§ Liliana Clemenza,‡,|| and David E. Isenman*,‡

Department of Biochemistry, University of Toronto, Toronto, Ontario, Canada M5S 1A8, and Department of Laboratory Medicine, University Hospital Malmö, Lund University, S-205 02 Malmö, Sweden

Received February 24, 2006; Revised Manuscript Received May 1, 2006

ABSTRACT: C4b-binding protein (C4BP) is a multimeric serum protein that is a potent regulator of the classical and lectin complement pathways. The binding site for C4b has been localized to complement control protein (CCP) domains 1−3 of the C4BP α-chain and, in particular, to a cluster of positively charged amino acids predicted to be at the interface between CCP 1 and CCP 2. To determine the regions of C4b contributing to C4BP binding, we have examined via surface plasmon resonance technology the binding of the C4c and C4dg subfragments of C4b to C4BP. At half-physiologic ionic strength, specific and saturable binding was observed for both C4c and C4dg. C4c exhibited much greater ionic strength sensitivity in its binding than did C4dg. Analysis of the effect on binding of the subfragments to various C4b-binding-defective C4BP mutants, together with cross-competition experiments, suggests that the subsites in C4BP for C4c and C4dg are adjacent, but distinct. Additionally, we observed synergy in subsite filling such that the presence of C4dg enhanced the extent of C4c binding over its basal level, and vice versa. The enhanced binding of C4c in the presence of C4dg was not due to an increase in affinity but rather reflected a 2−3-fold increase in the number of sites capable of binding C4c. This suggests the existence of a conformational equilibrium between high- and low-affinity states in the C4c binding subsite within each C4BP subunit, an equilibrium which is shifted in favor of the high-affinity state by the filling of the C4dg subsite.

The C3 convertase stages of the classical/lectin and alternative pathways of complement activation are the key points of amplification and effector function initiation in the complement system. Due to the potential for harm to host tissue, the complement system is stringently and redundantly regulated at these stages of complement activation. In humans, regulation is mediated by a family of proteins encoded in the RCA[1] (regulators of complement activation) locus on chromosome 1 (see ref *1* for a review of RCA protein structure and function). The family includes the soluble serum proteins factor H (fH) and C4b-binding protein (C4BP) and the host cell membrane-anchored proteins decay-accelerating factor (DAF), membrane cofactor protein (MCP), and complement receptors 1 and 2 (CR1 and CR2). With the exception of CR2, which does not function as a complement inhibitor, these proteins bind to the C4b or C3b subunits of the classical (C4b2a) and alternative (C3bBb) pathway C3 convertases and mediate their regulatory functionality by one or more of the following mechanisms: (1) accelerated dissociation of the C4b- or C3b-associated serine proteases C2a and Bb, respectively; (2) inhibition of the binding of intact C2 or factor B to C4b or C3b, respectively, thereby inhibiting the formation of new C3 convertases; and (3) acting as a cofactor for the cleavages mediated by factor I (fI), which irreversibly inactivates the C4b or C3b molecules as C3 convertase subunits.

Several pathogenic viruses targeting mammalian hosts express secreted regulatory molecules that display all three modes of C3 convertase regulatory mechanisms. The striking sequence similarity of these, particularly VCP (vaccinia control protein) and KCP/kaposica (Kaposi's sarcoma-associated herpes virus inhibitor of complement activation), to the mammalian complement regulatory proteins strongly suggests that the genes encoding these viral proteins were captured from the mammalian host RCA locus during the evolution of the respective viruses (*2*−*5*).

C4b-binding protein (C4BP) is the major serum-resident regulator of classical pathway C3 convertase (*6*) and displays all three functional activities referred to above. Like all

† This work was supported by Grant MOP-7081 from the Canadian Institutes of Health Research (DEI) and by grants from the Swedish Foundation for Strategic Research (INGVAR) and the Swedish Research Council (AB).

* To whom correspondence should be addressed. Tel: 416-978-2703. Fax: 416-978-8548. E-mail: d.isenman@utoronto.ca.

‡ University of Toronto.

§ University Hospital Malmö, Lund University.

|| Present address: Division of Experimental Therapeutics, Ontario Cancer Institute, 610 University Ave., Toronto, Ontario, Canada M5G 2M9.

[1] Abbreviations: C4BP, C4b-binding protein; CCP, complement control protein module; CR, complement receptor; DAF, decay accelerating factor; fH, factor H; fI, factor I; FPLC, fast protein liquid chromatography; KCP, Kaposi's sarcoma-associated herpes virus inhibitor of complement activation; MCP, membrane cofactor protein; MG, macroglobulin domain; RCA, regulators of complement activation; RU, resonance units; SPR, surface plasmon resonance; VCP, vaccinia control protein.

10.1021/bi0603827 CCC: $33.50
Published on Web 06/15/2006

members of the RCA family, the protein is comprised of multiple copies of an approximately 60-residue motif alternatively referred to as CCP (complement control protein) or SCR (short consensus repeat) domains. These domains have a common β-sheet framework that is stabilized by a pair of absolutely conserved disulfide bonds. The β-sheets are organized into layers forming a hydrophobic core but also have exposed loops of variable length (*1*). C4BP is unique among the RCA proteins in being a polymer and therefore intrinsically multivalent. Specifically, the major human plasma isoform is comprised of seven identical α-chains, each containing eight CCP domains, and one β-chain, which contains three CCP domains (*6*). Each class of chain has a C-terminal extension that mediates formation of a disulfide-linked, spider-like, polymer. The β-chain is dispensable for both C4b-binding function and polymerization, and indeed functionally active recombinant human C4BP consists only of six α-chains (*7*). Although each α-chain possesses an independent C4b-binding site, ultracentrifugation studies suggest that at physiologic ionic strength maximally four C4b molecules can be bound to any given C4BP molecule, likely due to steric constraints (*8*). Domain deletion analyses of the C4BP α-chain have revealed that CCP 1−3 is the minimal unit for expression of the regulatory functionality of the intact molecule (*7*). Like most RCA protein family member interactions with their ligands, that between C4BP and C4b is sensitive to ionic strength, suggesting an important role for ionic interactions (*8*, *9*). A model of the structure of the C4BP α-chain domains was built on the basis of the NMR coordinates of a pair of fH domains (*10*). A prominent feature of this model was a cluster of positively charged residues at the CCP 1−CCP 2 interface that included R39, K63, R64, and H67. Subsequent site-directed mutagenesis work confirmed the involvement of this positive patch in C4b binding and C4BP functionality (*9*, *11*, *12*). C4BP also binds polyanions such as heparin, and in fact, heparin binding is inhibitory to C4b binding (*9*). Consistent with this, the positively charged patch of residues shown to be important for C4b binding appears to be a major contact point for heparin, as well as other polyanions such as DNA (*9*, *13*). The structure of CCP 1−2 of the C4BP α-chain was recently solved by NMR, and it was found that the positively charged groups critical for binding of heparin, DNA, and C4b form a discontinuous surface extending over both modules (*14*). This implied that a binding-associated intermodular rotation would be required to bring all of the residues identified through mutagenesis to the same face of the molecule. Indeed, evidence for such a reorientation was inferred from NMR chemical shift perturbation experiments using a peptide derived from streptococcal M-protein that binds to a site overlapping the one for C4b (*14*).

For some of the RCA proteins, and their viral homologues, the contributions of the C3c/C4c and C3d(g)/C4d(g) fragments to the binding are known. For example, binding of C3c and C4c, but not C3d or C4dg,[2] to CR1 has been demonstrated (*15*−*17*). fH, which consists of 20 CCP domains, appears to have three distinct C3b binding sites (*18*, *19*). The first, consisting of CCP 1−4, binds only intact C3b (*19*), and these domains can on their own fully regulate a fluid phase alternative pathway C3 convertase (*20*−*22*). Regulation of a surface-bound alternative pathway C3 convertase requires the additional two C3b binding sites and their partially overlapping polyanion binding sites (*23*). Whereas C3b binding site 2, which has been broadly localized to CCP 8−15, can directly bind the C3c subfragment, C3b binding site 3, comprised of CCP 19−20, has the complementary subfragment specificity of being able to directly bind to the C3d region (*19*). For CR2, whereas there is agreement that C3d(g) on its own can mediate a strong interaction (*24*−*26*), there is some controversy about whether the respective binding affinities for CR2 of C3dg and iC3b, the latter containing both C3c and C3dg, are (*25*−*27*) or are not (*28*) essentially equivalent. However, using surface plasmon resonance (SPR) as the detection technique, a weak binding interaction between C3c and CR2 has been directly observed (*29*). VCP represents an interesting case in that it binds both C3b and C4b at sites on VCP that are sufficiently overlapping that the prebinding of one ligand precludes the simultaneous binding of the other ligand (*30*). However, when the respective "c" and "dg" region subfragments were examined, it appeared that the binding was principally mediated by one of the two subfragments but that it was C3dg in the case of C3b binding and C4c in the case of C4b binding (*30*). For C4BP, an analytical ultracentrifugation study suggested a very weak interaction with C4c and none with C4dg (*8*). However, the experimental setup would have made it difficult to detect weak binding to C4dg. By contrast, SPR technology allows one to detect fairly weak interactions that require higher concentrations of fluid phase ligand than would have been practical in the earlier analytical ultracentrifugation experiments. In this study we have examined by SPR technology the binding of the C4c and C4dg subfragments, as well as the parent C4b molecule, to both recombinant wild-type C4BP and to the C4b-binding-defective mutants referred to above. The major finding of the study is that not only can binding of each subfragment be directly observed to seemingly adjacent, yet distinct subsites but that there is an apparent synergy in the filling of the subsites. Specifically, our data suggest the existence within each C4BP subunit of a conformational equilibrium between a high-affinity and a much lower affinity conformation in the C4c binding subsite, an equilibrium which is shifted in favor of the high-affinity state by the filling of the C4dg subsite.

EXPERIMENTAL PROCEDURES

Purified Proteins. Recombinant wild-type C4BP, consisting of a disulfide-linked hexamer of C4BP α-chains, its monomeric CCP 1−8 derivative, the single domain deletion mutants spanning CCP 1 through CCP 4 of polymeric C4BP, and the C4BP polymer single or combination point mutants R39Q, R64Q, R66Q, R64Q/R66Q, R39Q/R64Q/R66Q, K63Q, H67Q, K126Q/K128Q, and F144S/F149S were expressed and immunoaffinity purified as described previously (*7*, *9*, *11*, *31*). Native human C4 of mixed isotype was purified from 50−100 mL quantities of human plasma by the method of Dodds (*32*). C4 was treated with 1% (w/w) purified $C\bar{1}s$

[2] By analogy with the C3 fragment nomenclature, we refer to the fI cleavage-delimited C4d fragment as C4dg to indicate that it contains an NH_2-terminal 45-residue "g" segment and to distinguish it from the structurally defined α−α6 C4d molecule visible in the X-ray crystal structure (*37*). The latter corresponds in length to the C3d proteolytic limit fragment of the physiologic C3dg fragment generated as a result of fI-mediated cleavages.

(Advanced Research Technologies, San Diego, CA), and the resulting C4b was subsequently purified on a Mono Q HR 5/5 FPLC column (Amersham Pharmacaia, Baie D'Urfé, Quebec, Canada) using gradient conditions that allow the separation of C4b monomer from spontaneously formed disulfide-linked C4b dimer (*17*, *33*). fI (*34*) and C4BP (*35*) were purified from human plasma as described previously. C4c was obtained by digestion of C4b with fI (1:30 w/w) in the presence of plasma-derived C4BP (1:50 w/w) for 18 h at 37 °C. C4c was then separated from C4dg by purification on Mono Q FPLC, as previously described (*17*). Prior to their use in SPR experiments, in order to remove any oligomeric material present, C4b and C4c were further purified by FPLC gel filtration using a Superose 6 HR 10/30 column (Amersham Pharmacaia) equilibrated with 10 mM HEPES, 75 or 150 mM NaCl, and 3 mM EDTA, pH 7.2.

A C3 preparation that had been purified from human plasma (*36*) was found to have undergone proteolytic degradation to the C3b stage upon long-term storage. This material was used for subsequent conversion to C3c and C3dg by overnight digestion at room temperature with fI (1:100 w/w) and soluble CR1 (1:50 w/w, a kind gift from Avant Immunotherapeutics Inc., Needham, MA). The digestion mixture was separated on a Mono Q HR 5/5 FPLC column using previously described gradient conditions (*15*). Prior to use in SPR experiments, C3c was further purified by gel filtration on a Superdex 200 HR 10/30 FPLC column (Amersham Pharmacaia) equilibrated with 10 mM HEPES, 75 mM NaCl, and 3 mM EDTA, pH 7.2.

Recombinant C4dg of the C4B isotype was expressed in *Escherichia coli* (*37*) and purified according to the modified procedure described previously (*17*). Prior to use in SPR experiments, C4dg was further purified by FPLC gel filtration using a Superdex 200 10/30 column equilibrated with 10 mM HEPES, 75 or 150 mM NaCl, and 3 mM EDTA, pH 7.

Recombinant C3dg C1010A was expressed in *E. coli* and purified as previously described (*38*) except that, in place of DEAE-Sephacel, the first chromatographic step employed a column of CM-Sepharose Fast Flow (Amersham Pharmacaia) equilibrated with 10 mM sodium acetate, 20 mM NaCl, and 1 mM EDTA pH 5.5. Following extensive washing, the column was step eluted with the same buffer containing 0.4 M NaCl. Prior to use in SPR experiments, C3dg was subjected to gel filtration as described above for C4dg.

The purity of all protein preparations was assessed by SDS−PAGE. The concentrations of C3 and C4 fragments were determined spectrophotometrically at 280 nm using as extinction coefficients (1%, 1 cm) 8.2 for C4b and C4c, 13.6 for C4dg, 9.7 for C3b and C3c, and 12.6 for C3dg. The concentrations of the recombinant C4BP proteins were determined from amino acid composition analyses (*7*).

Surface Plasmon Resonance Measurements. SPR measurements were performed primarily on a Biacore X instrument, with some experiments being done on a Biacore 3000 instrument (Biacore, Piscataway, NJ) when it was desirable to be able to have three experimental flow cells in series with the control flow cell. The experiments were conducted at 25 °C in HEPES-buffered saline [10 mM HEPES, 3 mM EDTA, 0.01% (v/v) surfactant P-20 (Biacore), pH 7.2] containing either 75 mM NaCl (half-physiologic ionic strength) or 150 mM NaCl (physiologic ionic strength). P-20 surfactant was added to all samples to a concentration of 0.01% (v/v) prior to their use. Proteins were immobilized on CM5 biosensor chips (Biacore) using the amine coupling kit from Biacore according to the activation protocol of the manufacturer and with the control flow cell being subjected to activation and deactivation without added protein. Immobilizations of C4BP and its variants, or the C4 fragments, were done at protein concentrations of 20−40 μg/mL in 10 mM sodium acetate, pH 4.5, at a flow rate of 5 μL/min. Typically, a flow of 10−20 μL gave an immobilized protein level of 4000−6000 RU. In all SPR experiments, the net RU values displayed have been corrected for nonspecific binding of analyte to the carboxylated dextran surface of the chip, and for bulk effects due to the presence of high concentrations of protein in some analytes, by subtracting from the experimental sensorgram the sensorgram derived from the sham activated−deactivated control channel that is connected in series to the experimental channel.

SPR Equilibrium Binding Measurements. Wild-type or mutant C4BP variants were immobilized on CM5 biosensor chips as described above, and C4 fragments at various concentrations were employed as analytes. Injections of C4dg and C4c analyte solutions were at a flow rate of 20 μL/min for 1 min, followed by 2 min of buffer flow for dissociation. Because of the longer time required to reach a steady-state plateau than was the case for C4c or C4dg, the binding of intact C4b was measured using a flow rate of 5 μL/min, with analyte injections of 10 min, followed by 2 min of buffer flow for dissociation. For all analytes employed, the biosensor chip surface was regenerated with a 1 min pulse of 2 M NaCl. The steady-state (or pseudo-steady-state) plateau region RU signal change data were analyzed according to a one-site Langmuir binding model (eq 1) using MacCurvefit v.1.5.5 nonlinear regression software (Kevin Raner Software, Victoria, Australia):

$$\Delta RU = \frac{\Delta RU_{max}[\text{analyte}]}{K_D + [\text{analyte}]} \quad (1)$$

The equilibrium binding data were also displayed in Scatchard form according to eq 2, but the lines drawn through the data points were determined by insertion of the K_A and RU_{max} values determined in the nonlinear fit procedure into eq 2.

$$\frac{\Delta RU}{[\text{analyte}]} = K_A \Delta RU_{max} - K_A \Delta RU \quad (2)$$

In a variation of the above-described equilibrium binding experiments for C4c and C4dg to biosensor chip-immobilized recombinant wild-type C4BP, or its monomeric derivative CCP 1−8, binding curves were also obtained using variable concentrations of C4c in the presence of a constant concentration of C4dg in the analyte (1 mg/mL, 25 μM) or variable concentrations of C4dg in the presence of a constant concentration of C4c (54 μg/mL, 0.36 μM) in the analyte. The respective concentrations of the nonvaried component of the analyte mixtures corresponded to midrange response points of binding curves obtained with C4dg and C4c on their own. In each case, the net signal change due to the varied analyte protein was obtained after subtraction of the

sensorgram of the nonvaried component of the analyte on its own using the BIAevaluation 3.0 software (Biacore).

SPR Competition Experiments. Recombinant wild-type C4BP at a fixed concentration (typically 42 μg/mL, corresponding to 0.6 μM subunit sites) was injected over biosensor chip channels coupled with either C4dg or C4c. The C4BP was injected either on its own or after premixing with a potential fluid phase competitor of the binding such as C4dg, C4c, C4b, or C3dg. The analyte flow rate was 20 μL/min, the injection phase was for 1 min, and the protein competition experiments were all carried out in half-physiologic ionic strength buffer.

C4BP Mutant Scan SPR Experiment. Using a CM5 chip mounted in a Biacore 3000 instrument, C4b, C4c, and C4dg were immobilized as described above onto separate flow channels, with flow channel 1 serving as the sham activated−deactivated control for nonspecific binding. Recombinant wild-type and mutant polymeric C4BP, each at a concentration of 10 μg/mL, were injected at a flow rate of 20 μL/min for 1 min over all four flow channels that were connected in series, followed by a 1 min buffer flow dissociation phase. The experiments with each recombinant C4BP were performed at both physiologic and half-physiologic ionic strength conditions. The chip surfaces were regenerated between injections with a 1 min pulse of 2 M NaCl. The net signal change at the end of the injection phase was taken as a measure of relative binding strength, with all results being normalized to the RU change obtained at each of the two ionic strength conditions for recombinant wild-type C4BP.

Inhibition of C4BP Binding to C4 Fragments with Heparin. Various concentrations of heparin (Sigma-Aldrich, St. Louis MO) were preincubated with 10 μg/mL wild-type recombinant C4BP prior to injection over the above-described biosensor chip coupled on separate channels with C4b, C4c, and C4dg. The experiment was conducted at both half-physiologic and physiologic ionic strengths, with the heparin concentration range varying between 0.1−50 μg/mL and 0.5−10 mg/mL, respectively, for the two buffer conditions. The net signal change at the end of the 1 min injection phase was taken as a measure of relative binding strength, with all results being expressed as a percentage of the RU change obtained in the absence of heparin in the analyte.

RESULTS AND DISCUSSION

C4BP Binds both the C4c and C4dg Subfragments of C4b. As the extent of interaction between C4BP and C4b was known to increase at low ionic strength (*8*, *9*), our initial surface plasmon resonance experiments aimed at determining whether the C4c and C4dg subfragments of C4b bind to C4BP were carried out at half-physiologic ionic strength. To this end, wild-type C4BP was coupled to a CM-5 biosensor chip, and sensorgrams were obtained using incremental concentrations of C4b, C4c, and C4dg as analytes. In each case, the analyte protein had been exchanged into the SPR running buffer, and separated from any minor oligomeric species formed upon storage, by size exclusion chromatography within 24 h of its use. A representative SDS−PAGE analysis of the fragments employed for our SPR experiments is shown in Figure 1. As can be seen in Figure 2, binding data for the subfragments, as well as the parent

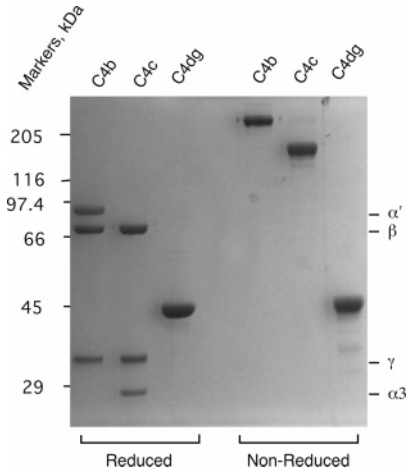

FIGURE 1: SDS−PAGE (9% gel) of the C4 fragments used in the SPR experiments. The fragments were analyzed under both reducing and nonreducing conditions, as indicated. The constituent chains of C4b and C4c are indicated, except for the ~16 kDa α4 fragment of C4c which is not resolved from the dye front on this percentage gel.

molecule, were readily obtained at half-physiologic ionic strength. Although the kinetics of binding, especially for the case of C4b as the analyte, would have been very complex to analyze because there are clearly fast and slow components to both the association and dissociation phases of the sensorgrams, the sensorgrams all approached an equilibrium state by the end of the injection phase. A plot of the RU values from the pseudoequilibrium plateaus of the respective pile-up sensorgrams (Figure 2, panels A−C) versus analyte concentration yielded saturation-type binding curves in each case that were reasonably well fit by a Langmuir binding model for a single class of binding site (Figure 2, panels D−F). It can further be seen from the Scatchard transformations of the data (Figure 2, panels G−I) that, for the case of both C4b and C4dg, the binding data conformed quite well to what would be expected for a single, noncooperative, class of binding site. Keeping in mind that the hexameric C4BP is likely to be covalently tethered to the biosensor chip by only one or two of its subunits and that such covalent coupling, as well as proximity to the carboxylated dextran surface, may affect the intrinsic affinity of a subunit for its partner protein, the derived K_D values in each case (see Figure 2 insets in panels D−F and Table 1) no doubt reflect an average among the subunits. Nevertheless, the spread in affinities must be narrow enough that separate classes of binding sites are not readily apparent. With C4c as the analyte, we fairly consistently saw some deviation from single class of site behavior on the Scatchard transformations of the data (Figure 2H). Although the quality of the fit was always improved by invoking a two classes of binding site model, there were usually not enough data points within the concentration range required by at least one of the classes of binding site, and consequently very large error estimates for the parameters, to justify acceptance of the fit parameters derived using a two-site model. As discussed further below, the heterogeneity in binding behavior of C4c is likely real, but for the purpose of comparing binding parameters between mutant and wild-type C4BP molecules, or the reproducibility among replicate experiments, the fit parameters of the single class binding site model have been reported in Table 1.

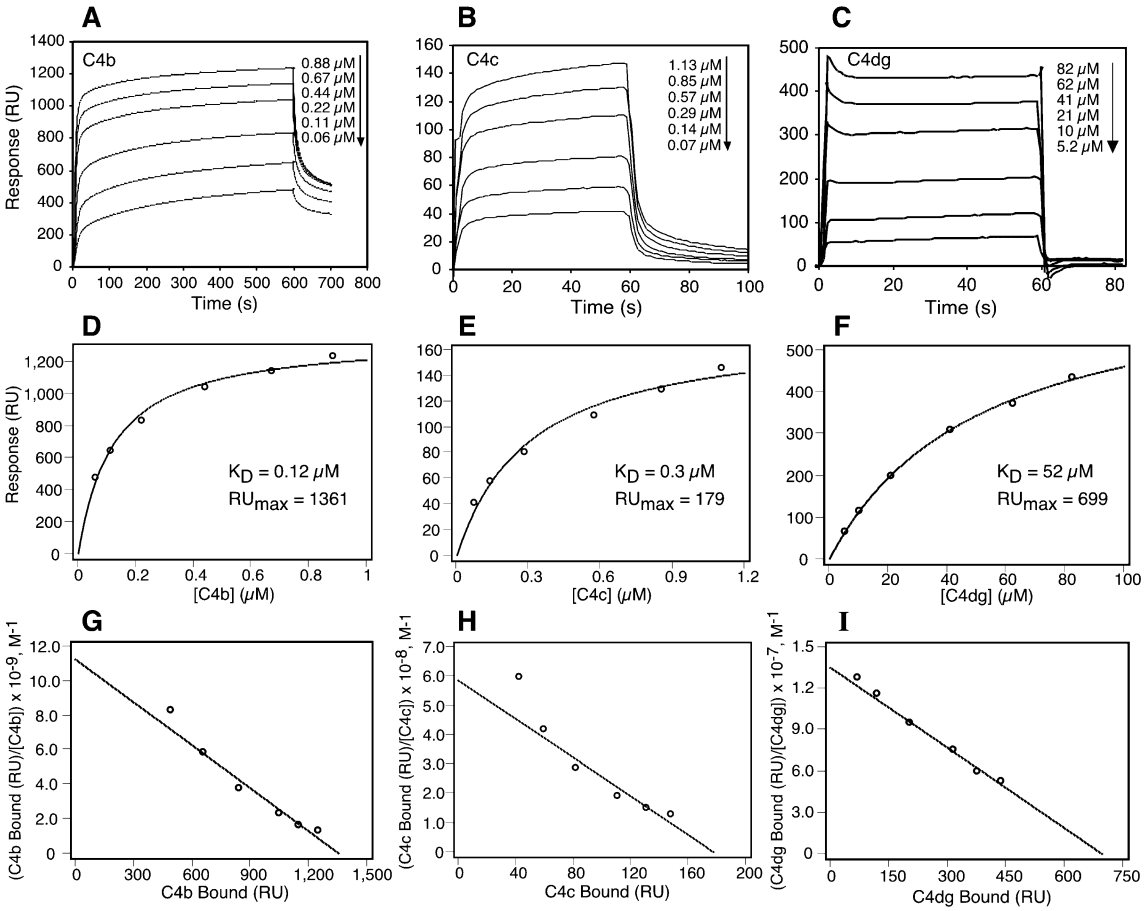

FIGURE 2: SPR analysis of the interaction of C4b, C4c, and C4dg with biosensor-coupled wild-type C4BP. Sensorgram overlay plots of net RU change above that of the control channel when analyte solutions of varying concentrations of C4b (panel A), C4c (panel B), and C4dg (panel C) were flowed over a biosensor channel coupled with ~4500 RU of recombinant wild-type C4BP. The analyte concentrations corresponding to each set of sensorgrams are indicated to their right in descending order of concentration. Whereas the C4b injections were for 600 s at a flow rate of 5 μL/min before the changeover to buffer flow, those of C4c and C4dg were for 60 s at a flow rate of 20 μL/min. The experiments were all conducted in half-physiologic ionic strength HEPES buffer. Panels D−F display the steady-state plateau level RU changes due to specific binding for the individual sensorgrams as a function of analyte concentration for C4b, C4c, and C4dg, respectively. The binding curves were fit by nonlinear regression according to the equation for a single class of binding site (eq 1, Experimental Procedures). The values of K_D and RU_{max} for these single representative experiments are given in the respective panels, with means and standard deviations of replicate experiments being presented in Table 1. Panels G−I show the binding data in Scatchard form for C4b, C4c, and C4dg, respectively. The lines drawn represent the insertion into eq 2 of Experimental Procedures of values for K_A and RU_{max} determined from the nonlinear fit procedure used in panels D−F.

Given that 4500 RU of C4BP were initially coupled to the biosensor chip, the mean RU_{max} (resonance units change at saturating concentrations of analyte) value for C4b binding of 1253 represents ~10% of the theoretical maximum based upon every 70 kDa subunit of C4BP binding one C4b molecule (190 kDa). Even for this level of accessible C4b-binding sites on the chip, based on the relative molecular masses of monomeric C4b and C4c (~150 kDa), the expected RU_{max} for C4c should be ~990. Thus, the mean RU_{max} value of 209 observed when C4c was used as the analyte represents ~20% of the expected value. The mean affinity of C4c for these binding sites was 0.2 μM, which is only 2−3-fold weaker than was observed with intact C4b (0.07 μM K_D; see Table 1). By contrast, the relatively weakly binding C4dg fragment (mean K_D of 53 μM) displays a RU_{max} of 678, more than twice the value of 266 predicted from the relative molecular masses of C4dg (40.4 kDA) vs C4b. This is likely due to the much smaller C4dg fragment having greater access to C4BP subunits on the chip than would be the case for either intact C4b or C4c.

Ionic Strength Dependence of the Binding. When binding to a C4BP-coupled biosensor chip was analyzed at physiologic ionic strength, saturation-type curves were obtainable for C4b and C4dg, which were well described by the Langmuir binding isotherm for a single class of binding site (Figure 3). For C4c, however, using analyte concentrations up to 1 μM, only the early pseudolinear portion of the binding curve was obtained and was therefore not suitable for quantitative analysis (data not shown). The ionic strength dependence of the interaction between C4b and C4BP is seen in Figure 3A, there being an ~45% decrease in both affinity and RU_{max} in going from half-physiologic to physiologic ionic strength (Table 1). The significantly higher RU_{max} observed at the lower ionic strength may reflect the previously reported increase in stoichiometry from 4 to 6 C4b per C4BP molecule that was deduced from analytical ultracentrifugation experiments carried out at physiologic and half-physiologic ionic strengths (*8*). In contrast to the ionic strength sensitivity of the interactions of C4BP with C4b and C4c, the binding curves obtained using C4dg as the

Table 1: Binding Parameters Determined from SPR Measurements for the Interaction of Wild-Type and Selected Mutant C4BP Molecules with C4b, C4c, and C4dg

ligand coupled	RU coupled	[NaCl] in analyte buffer, M	analyte	K_D, μM	RU_{max}	no. of expts[a]
C4BP WT	4500	0.075	C4b	0.07 ± 0.04	1253 ± 99	3
	4500	0.075	C4c	0.2 ± 0.1	209 ± 27	3
	4500	0.075	C4dg	53 ± 12	678 ± 78	4
C4BP WT	5700	0.075	C4b	0.15	1005	1
	5700	0.15	C4b	0.27	568	1
	5700	0.075	C4dg	79	699	1
	5700	0.15	C4dg	113	874	1
C4BP H67Q	5200	0.075	C4b	0.45 ± 0.19	96 ± 8	3
	5200	0.075	C4c	unmeasurable		3
	5200	0.075	C4dg	88.7 ± 19.2	261 ± 33	3
C4BP F144S/F149S	4200	0.075	C4b	0.09	740	1
		0.075	C4c	0.14	419	1
		0.075	C4dg	94	495	1
C4BP R66Q	5200	0.075	C4b	0.11	1169	1
		0.075	C4c	0.28	224	1
		0.075	C4dg	46	777	1

[a] The number of separate experiments used in determining means and standard deviations for K_D and RU_{max} is indicated in the last column. In all experiments, including those shown for which replicates are not presented, the error estimates of the nonlinear fit of the data were consistently ≤20% for each of the two fitted parameters.

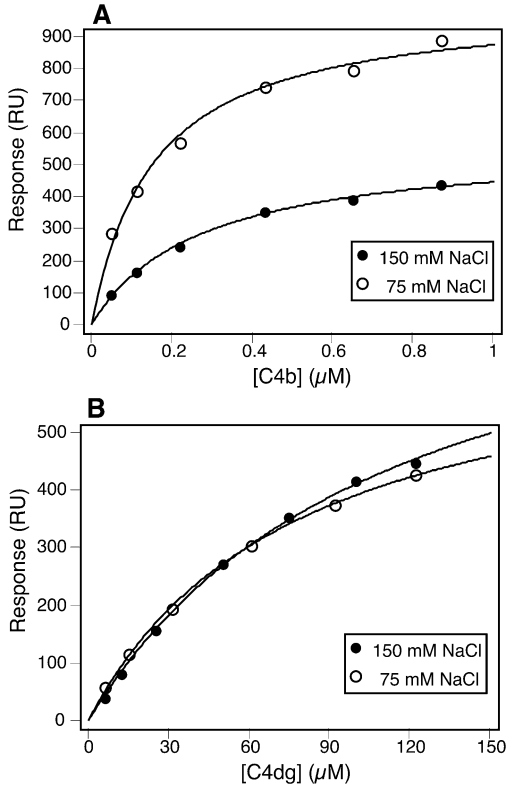

FIGURE 3: Ionic strength dependence of the binding of C4b and C4dg to wild-type C4BP. SPR analyses as described in Figure 1 were carried out to monitor the steady-state plateau levels of binding of variable concentrations of C4b (panel A) and C4dg (panel B) to a recombinant wild-type C4BP-coupled biosensor chip (5700 RU) in physiologic (closed circles) and in half-physiologic (open circles) ionic strength HEPES buffer. The binding curves were fit by nonlinear regression according to the equation for a single class of binding site (eq 1, Experimental Procedures). The values for K_D and RU_{max} are reported in Table 1.

ligand were quite similar at physiologic and half-physiologic ionic strength (Figure 3B, Table 1). This observation does not preclude an ionic component to the binding of C4dg to C4BP as it may reflect the net result of two opposing effects, namely, the ionic interactions being weakened in going from 75 to 150 mM NaCl but the hydrophobic interactions being strengthened. A further indication that the binding of C4c to C4BP was more sensitive to ionic strength conditions than was either C4dg or the intact C4b molecule came from an experiment in which intact hexameric C4BP was used as the analyte at a single concentration of 10 μg/mL, and binding to biosensor surfaces coupled with C4b, C4c, and C4dg was assessed at both half-physiologic and physiologic ionic strength. On the C4c channel the binding at physiologic ionic strength was >100-fold lower than that at half-physiologic ionic strength (3 vs 380 RU). By contrast, on the C4dg channel, the binding at the higher ionic strength was ~3-fold less than that at half-physiologic ionic strength (580 vs 1800 RU). Binding to the C4b channel under these multipoint attachment conditions was approximately the same at both ionic strengths (1700 RU).

Assessment of the Specificity of the Binding Interactions with the C4b Subfragments. Despite not being of the expected magnitude with respect to RU_{max}, the interaction observed between C4c and C4BP was not unanticipated, based upon indications of it in the earlier solution study (*8*). Since the relatively weak interaction with C4dg was novel, it was important to perform additional specificity controls. To this end, C4dg was coupled to the biosensor chip, and the hexavalent recombinant wild-type C4BP was employed as the analyte. We hypothesized that if the binding interaction between C4BP and C4dg was specific, then preincubation of the analyte C4BP with C4dg prior to flowing it over the C4dg-coupled chip should inhibit analyte binding. As can be seen in Figure 4A, whereas injection of C4BP at a concentration of 42 μg/mL (~0.6 μM sites) over the C4dg-coupled chip gave a signal change of ~2100 RU at the end of the 60 s injection phase, the same concentration of C4BP preincubated with C4dg at 1 mg/mL (25 μM) decreased the maximal signal change to ~600 at the end of the injection phase. Intermediate concentrations of C4dg as the fluid phase competitor gave rise to a dose-dependent inhibition response (data not shown). As an additional control to show that the inhibition seen was not due to overcorrections for the large bulk effect signal changes in both the experimental and control channels brought about by using protein concentra-

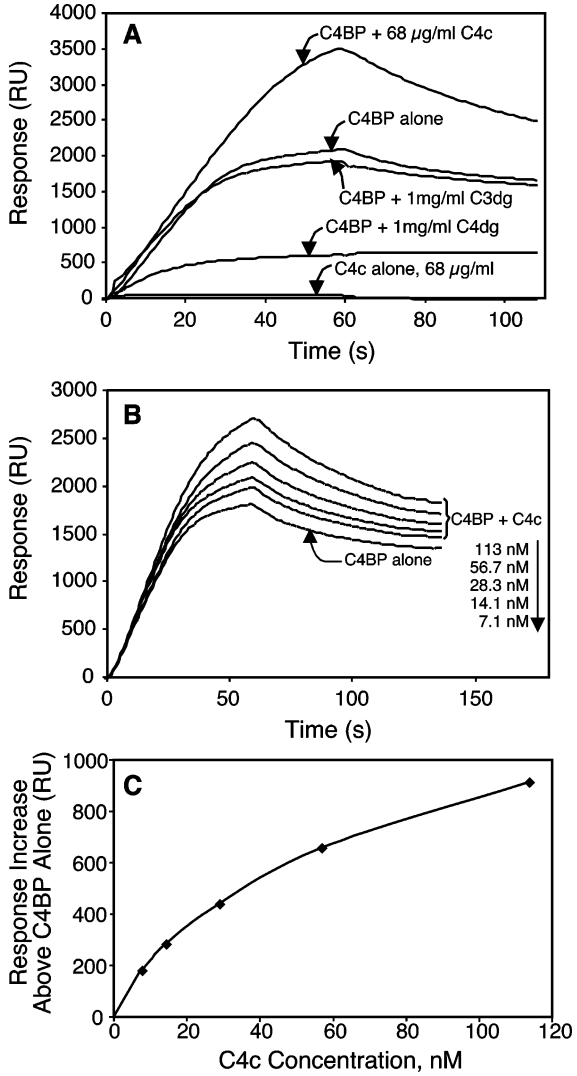

FIGURE 4: Effect of preincubation with potential fluid phase competing ligands on the ability of recombinant wild-type C4BP to bind to a C4dg-coupled biosensor chip. (A) SPR sensorgrams monitoring the binding of 42 μg/mL recombinant wild-type C4BP to a biosensor chip bearing ~5000 RU of C4dg in the absence and presence of the indicated concentrations of fluid phase C4dg, C3dg, and C4c. C4c, at the same concentration as in the preincubation experiment, was also injected in the absence of C4BP. Analyte injection was for 60 s at 20 μL/min before switching to buffer flow. All experiments were carried out in the half-physiologic ionic strength HEPES buffer. (B) Sensorgrams showing the dose-dependent enhancement in the binding of C4BP (42 μg/mL, or 0.6 μM subunit sites) to the C4dg surface as a function of C4c concentration premixed with the C4BP analyte. The concentrations of C4c in the analyte are indicated in descending order to the right of the series of sensorgrams. (C) The change in RU values at the end of the injection phase minus the signal due to C4BP binding alone is plotted as a function of the C4c concentration in the analyte.

tions in excess of 1 mg/mL, the standard 42 μg/mL concentration of C4BP was preincubated with 1 mg/mL C3dg, a fragment of very similar molecular weight to C4dg and having the same fold but different surface charge distribution (*37*). This resulted in a response curve that was nearly indistinguishable from that of C4BP alone (Figure 4A). On one hand, this showed that the bulk effect signal changes were being accurately corrected for, and on the other hand, it indicated that C3dg had no measurable binding affinity for C4BP. Finally, binding of C4BP to the C4dg-coupled chip was inhibited by intact C4b in a dose-dependent manner and over a concentration range commensurate with its higher intrinsic affinity for C4BP relative to C4dg (data not shown).

We next asked whether the C4c and C4dg binding sites overlap by determining whether preincubation of C4BP with C4c (68 μg/mL, 0.45 μM) would inhibit the binding of C4BP to the C4dg-coupled biosensor chip. Far from inhibiting the binding, it can be seen in Figure 4A that the preincubation step with C4c resulted in an ~1.7-fold increase (~1400 RU change) in binding signal at the end of the injection phase. That this was not due to a direct binding of C4c to the C4dg-coupled chip was demonstrated through a control injection of 68 μg/mL C4c alone over the chip. As seen in Figure 4A, this gave rise to a very small increase in net signal (~67 RU). The enhancement in C4BP binding to the C4dg-coupled chip by C4c was dose-dependent and showed characteristics of a saturation curve if the enhancement in RU over the basal C4BP binding seen at the end of the injection phase was plotted as a function of C4c concentration (Figure 4B,C). No quantitative analysis of Figure 4C was undertaken because, first, the values plotted do not represent an equilibrium binding level and, second, multivalent C4BP binding to a surface array of C4dg would not be expected to follow any simple binding model.

The above data suggest that C4c is being carried along with C4BP when the latter binds to the C4dg-coupled chip. One possibility to be considered is that C4c binds predominantly to C4BP subunits that do not bind to the biosensor chip-associated C4dg molecules. If this were the case, however, the dissociation phase kinetics should initially be rapid, similar to what was observed in Figure 2B when C4c was the analyte being flowed over a C4BP-coupled biosensor chip. Dissociation should then level off into a slow kinetic phase at an RU level corresponding to that for C4BP by itself, which dissociates very slowly due to its multivalent attachment to C4dg on the biosensor chip. Instead, relatively slow dissociation kinetics were observed throughout, thus negating the unoccupied subunit possibility for the RU enhancement observed in the presence of C4c. An alternative explanation is that the C4c and C4dg binding sites are adjacent, but nonoverlapping, and that they act synergistically if both sites are filled at the same time. Whether through induced conformational effects on the binding interface or otherwise, coligation of the adjacent C4c and C4dg sites results in enhanced binding of C4c. The relatively slow dissociation phase of the C4c-dependent enhancement in signal could have a number of origins, ranging from an enhancement in the affinity of C4c for its subsite when the C4dg subsite is simultaneously occupied to the more trivial explanation that C4c is sterically impeded from dissociating from its subsite due to the cage-like nature of the multivalent binding of C4BP subunits to C4dg on the biosensor chip. These issues will be addressed further in experiments presented below in which C4BP is coupled to the biosensor chip and C4c and C4dg are used as coanalytes. However, before leaving the issue of competitive ligands, the sensorgrams presented in Figure 5 indicate that when C4c is the entity coupled to the chip, the binding of C4BP can be inhibited by preincubation with C4c, C4dg, and C4b. In a control experiment, C3dg preincubated with C4BP at the same concentration used for inhibition by C4dg did not affect the binding of C4BP to C4c (Figure 5). The fact that C4dg can inhibit the binding

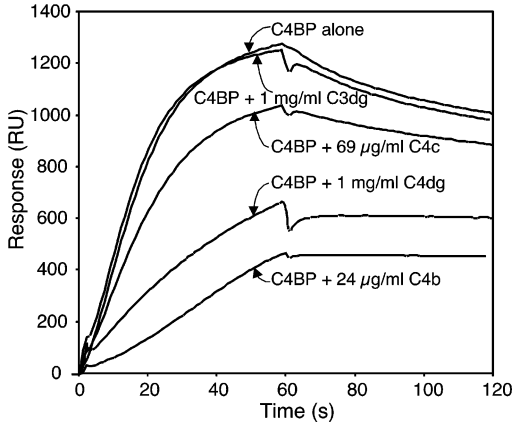

FIGURE 5: Effect of preincubation with potential fluid phase competing ligands on the ability of recombinant wild-type C4BP to bind to a C4c-coupled biosensor chip. A fixed concentration of recombinant wild-type C4BP (42 μg/mL) was injected over a C4c-coupled biosensor chip (~4700 RU) alone or in the presence of the indicated concentrations of C4c, C4dg, C3dg, or C4b. Analyte injection was for 60 s at 20 μL/min before switching to buffer flow. All experiments were carried out in the half-physiologic ionic strength HEPES buffer.

of C4BP to a C4c chip, whereas C4c cannot inhibit C4BP binding to a C4dg chip, suggests that the order of subsite occupancy may determine the outcome.

Synergy of C4c and C4dg Binding to C4BP. To better determine whether there was synergy between the C4dg and C4c subsites, the experimental design needed to be changed to avoid the complicating effects of multivalent attachment to the ligand on the biosensor surface. The test system involved coupling C4BP to the CM5 chip and then comparing the binding curves derived from the steady-state plateau regions when C4c alone was the analyte versus the same range of C4c analyte concentrations that had been premixed with a constant concentration of C4dg. The signal increase due to C4dg binding on its own would then be subtracted from the plateau values resulting from injection of the various C4c/C4dg mixtures. Panels A and B of Figure 6 respectively display on the same scale the sensorgrams from a series of identical C4c analyte concentrations injected over the same C4BP-coupled chip, either in the presence of 1 mg/mL C4dg (25 μM) or alone. The sensorgram generated by the 1 mg/mL C4dg on its own is also shown (Figure 6A). The enhancement in C4c binding is readily apparent even in these primary data. Shown in Figure 6C are the corresponding steady-state plateau-derived C4c binding curves in which the signal change due to C4dg binding has been subtracted from the data. The simplifying assumption made here is that the signal change reflecting C4dg binding is constant, but there is some experimental evidence for this given below (Figure 6E,F). The data sets in Figure 6C have each been fit to a single class binding site model, and they are also shown as Scatchard transformations in Figure 6D. As is readily apparent from the near parallel nature of the lines of the Scatchard plots, the presence of C4dg has a minimal effect on the affinity of C4c binding to C4BP but increases the number of sites having this affinity by ~3-fold (see also Table 2).

The reciprocal experiment was also performed in which C4dg was the varied analyte and C4c was held constant at a concentration of 0.36 μM. The direct binding isotherm fits for this experiment, as well as their Scatchard transformations, are shown in panels E and F of Figure 6, respectively. It can be seen that in this case, after subtracting out the signal due to C4c binding on its own, the primary effect of having C4c present is to increase the apparent affinity of C4dg binding by approximately 8-fold, while having a very minimal effect on the maximal number of C4dg binding sites (see also Table 2).

Coupling of intact hexavalent C4BP to the biosensor chip, followed by flowing monovalent analyte over it, as was done for the experiments depicted in Figure 6, should have resulted in an intrinsic affinity situation, despite the multivalent nature of C4BP. Formally, however, one cannot exclude the possibility of intersubunit allosteric cooperativity accounting for the synergistic effects of C4c and C4dg subsite filling that we have observed. For this reason, experiments similar to those described above were performed using a biosensor chip to which we had coupled a monomeric form of C4BP consisting of CCP 1−8 but lacking the COOH-terminal polymerization segment. As is readily apparent in Figure 7 (panels A and B), the presence of a constant amount of C4dg (25 μM) still resulted in a substantial enhancement in the number of C4c binding sites at saturation when C4c was the varied analyte, with little change in affinity (see also Table 2). Similarly, when C4dg was the varied analyte, the presence of a constant concentration of C4c (0.36 μM) increased the affinity of binding, without substantial effect on the maximal number of binding sites for C4dg (Figure 7C,D; see also Table 2). Thus the observed C4dg/C4c synergies of binding are autonomous to a single C4BP subunit. Finally, shown in Figure 7 are the results of additional specificity controls in which the C4c and C4dg titrations were respectively carried out in the presence of 25 μM C3dg (in place of 25 μM C4dg) and 0.36 μM C3c (in place of 0.36 μM C4c), as the nonvaried analytes. It can be seen that the resultant binding curves, and binding parameters (Table 2), were nearly identical to those obtained for C4c and C4dg on their own.

C4c and C4dg Share Some Common Contact Residues within the Positively Charged Cluster at the CCP 1−CCP 2 Interface. We wished to determine the effect, if any, on C4b subfragment binding to a series of mutant C4BP molecules that had previously been found to be defective to varying degrees with respect to their C4b-binding, decay−acceleration, and fI−cofactor activities (*9*, *11*, *12*, *31*). The series included both single and combination mutations to glutamine within a cluster of basic residues (R39, K63, R64, R66) at the interface between CCP 1 and CCP 2 in the homology-modeled structure of the C4BP α-chain. We also tested several additional point mutants within CCP 2 (H67) and CCP 3 (K126, K128, F144, F149) and single domain deletion mutants covering CCPs 1−4. As all of the mutants had previously been shown to form disulfide-liked multimers comparable to those of recombinant wild-type C4BP, the experimental design involved flowing the variant forms of C4BP at a constant concentration of 10 μg/mL over flow channels coupled with C4b, C4c, or C4dg. Since in these experiments a steady-state plateau level is not reached within the 60 s injection period due to the complex kinetics of multivalent binding (see Figures 4A,B and 5 for examples of this), we have taken the RU change at the end of the injection phase as a rough measure of the relative binding

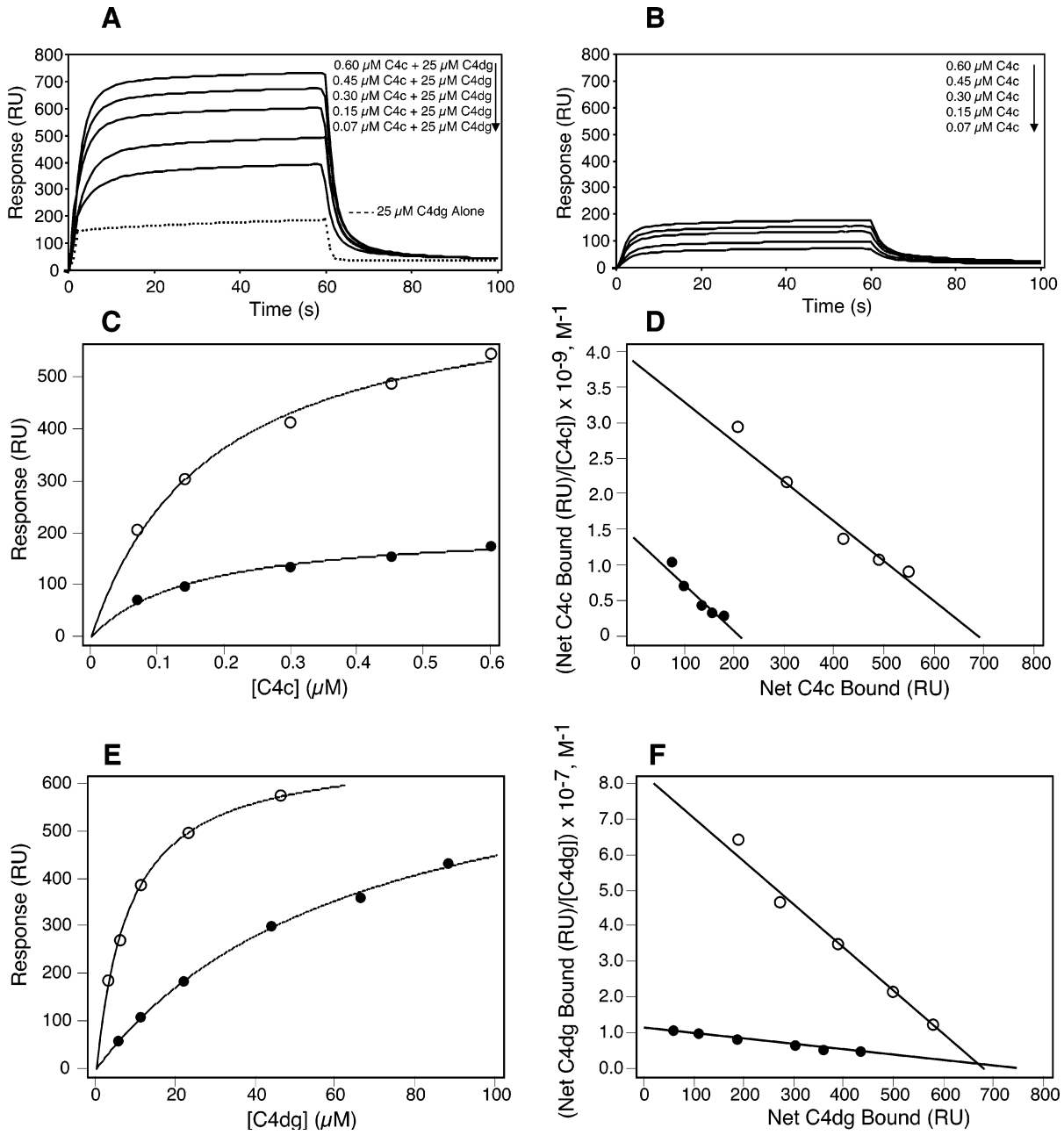

FIGURE 6: Synergy of C4c and C4dg binding to wild-type C4BP. SPR sensorgram overlays of variable analyte concentrations of C4c (indicated in descending order to the right of the sensorgrams) binding to immobilized recombinant wild-type C4BP (4500 RU) either on its own (panel B) or when the analyte C4c was premixed with 25 μM C4dg (panel A). The signal change due to 25 μM C4dg on its own is indicated (dashed trace, panel A). The experiment was carried out in half-physiologic ionic strength HEPES buffer. Panel C depicts the direct binding curves derived from the steady-state plateau data in panel B (open circles) and from panel A after subtraction of the signal change due to C4dg on its own (closed circles). The same data in Scatchard transformation form are shown in panel D. The data were analyzed according to the one class of site binding model (eq 1, Experimental Procedures), and as before, the lines on the Scatchard plots are drawn according to the parameters derived from the nonlinear fit of the data. Panels E (direct binding) and F (Scatchard transformation) represent data obtained on the same chip from an experiment in which the concentration of C4dg in the analyte was varied in the absence (closed circles) or presence (open circles) of a fixed concentration (0.36 μM) of C4c. The signal change due to C4c binding on its own has been subtracted in the latter case. The K_D and RU_{max} values from these experiments are reported in Table 2.

activities of the mutant forms of C4BP to C4b and its constituent subfragments. The binding activities from one such mutant scan experiment, normalized in each case to wild-type activity, are shown in Figure 8. In this experiment, C4b, C4c, and C4dg were coupled to separate channels on the same biosensor chip and therefore were exposed to exactly the same concentration of any given analyte. The experiment was conducted at both physiologic and half-physiologic ionic strength; however, in the case of the C4c channel, only the half-physiologic ionic strength data are shown as very little binding to C4c was seen even for the wild-type protein at physiologic ionic strength. The physiologic ionic strength data on the C4b channel (Figure 8A) permit comparisons for this series of mutants to earlier ELISA plate-based binding data in the literature (*7*, *9*, *11*). Consistent with the earlier data, deletion of any of CCP domains 1−3, as well as mutations involving most of the basic residues at the modeled CCP 1−CCP 2 interface, or on the same face of CCP 2, had a deleterious effect on binding that was generally more apparent at physiologic ionic

Table 2: Effect of the Presence of the Complementary C4b Subfragment on the SPR-Determined Binding Parameters for the Interaction of C4c and C4dg with Wild-Type C4BP or CCP 1−8 Monomer

ligand coupled	RU coupled	nonvaried analyte/ concn, μM	varied analyte	K_D, μM	RU_{max}	affinity[a]	RU_{max}[a]
C4BP WT	4500		C4c	0.16	214		
	4500	C4dg/25	C4c	0.18	692	0.9	3.2
C4BP WT	4500		C4dg	67	750		
	4500	C4c/0.36	C4dg	8.3	680	8.1	0.9
C4BP CCP 1−8	2400		C4c	0.28	79		
	2400	C4dg/25	C4c	0.49	210	0.6	2.7
	2400	C3dg/25	C4c	0.36	94	0.8	1.2
C4BP CCP 1−8	2400		C4dg	72	238		
	2400	C4c/0.36	C4dg	20	212	3.6	0.9
	2400	C3c/0.25	C4dg	80	254	0.9	1.1

[a] Relative to the basal level in the presence of nonvaried analyte.

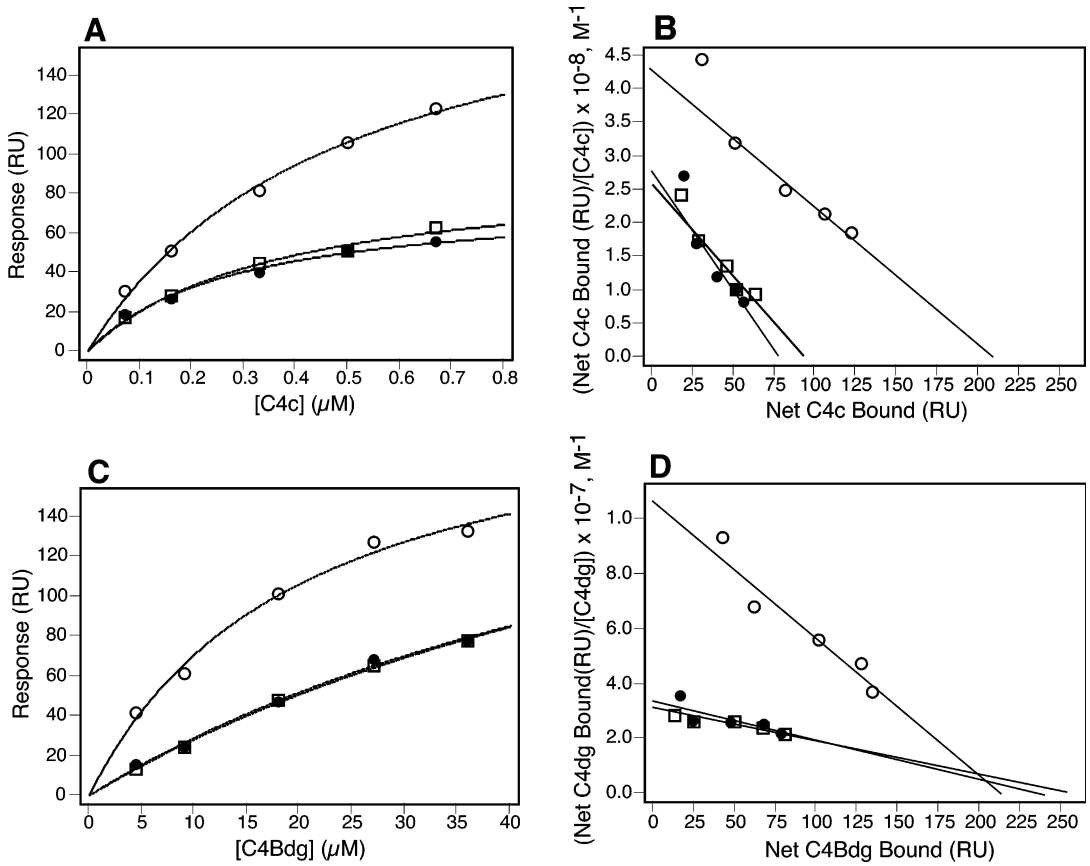

FIGURE 7: Synergy of C4c and C4dg binding to the CCP 1−8 derivative of C4BP. Similar to the experiments depicted in Figure 6, variable concentrations of C4c were injected over a biosensor chip bearing 2400 RU of the CCP 1−8 monomer version of C4BP in the absence (closed circles) or presence of 25 μM C4dg (open circles) or 25 μM C3dg (open squares). Direct steady-state plateau-derived binding curves, after subtraction of signal due to the nonvaried analyte on its own, are depicted in panel A and as Scatchard transformations in panel B. Panels C (direct binding) and D (Scatchard transformation) represent data obtained on the same chip from an experiment in which the concentration of C4dg in the analyte was varied in the absence (closed circles) or presence (open circles) of a fixed concentration (0.36 μM) of C4c or C3c (open squares). The signal change due to C4c binding on its own has been subtracted; C3c on its own gave no signal change. The K_D and RU_{max} values from these experiments are reported in Table 2. The experiments were carried out in half-physiologic ionic strength HEPES buffer.

strength than at half-physiologic ionic strength. Of the domain deletion mutants, the one lacking CCP 2 is the most severely compromised, consistent with the fact that residues K63, R64, and H67, all of which as point mutants show defective binding to C4b in our surface plasmon resonance experiments at physiologic ionic strength (Figure 8A), are located in CCP 2. The CCP 4 domain deletion, as well as the R66Q single residue mutation, was without effect on C4b binding (Figure 8A), similar to what had been reported previously (*7*, *12*). The same was true for double residue mutants K126Q/K128Q and F144S/F149S of the CCP 3 domain, both of which had previously been shown to display normal, or even slightly enhanced, C4b binding but severely impaired fI−cofactor activity (*31*).

The results obtained for the series of mutants flowed over the C4c and C4dg channels are shown in panels B and C of Figure 8, respectively. In general, most of the mutants that showed defective binding to C4b at physiologic ionic strength showed a substantially greater level of defect in binding to both C4c and C4dg, even at half-physiologic ionic strength. One notable exception to this generality was the H67Q mutant, which showed less than 10% of wild-type binding

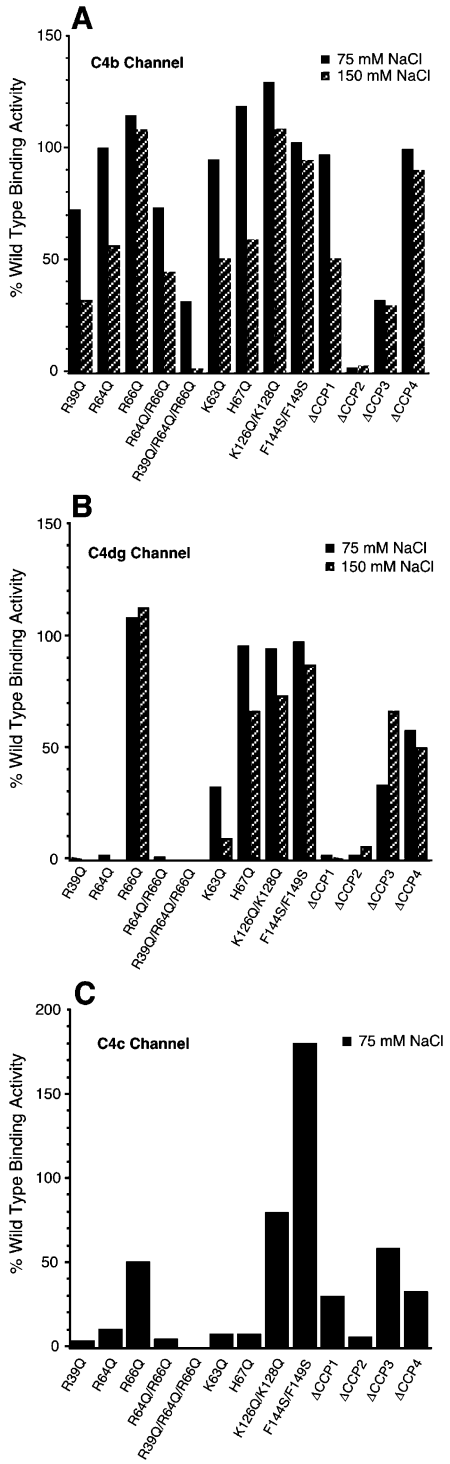

FIGURE 8: Relative binding activity of a series of amino acid substitution, and CCP domain deletion, mutants of C4BP to immobilized C4b, C4dg, or C4c. The data were collected on a Biacore 3000 instrument in which recombinant wild-type or mutant C4BP polymers, all at a concentration of 10 μg/mL, were injected over a sham activated−deactivated control channel connected in series with channels bearing C4b (~5900 RU, panel A), C4dg (~7100 RU, panel B), or C4c (~5000 RU, panel C). The net signal change at the end of the 60 s, 20 μL/min injection phase for the wild-type protein was defined as 100% binding, and the results with all mutants were expressed as a percentage of wild-type activity. Solid bars represent experiments conducted in half-physiologic ionic strength HEPES buffer, and hatched bars represent experiments conducted in physiologic ionic strength HEPES buffer. Binding to C4c was not measurable at physiologic ionic strength for even wild-type C4BP.

activity to C4c but near wild-type binding to C4dg at half-physiologic ionic strength and ~70% of wild-type binding at the more stringent physiologic ionic strength condition. Binding of mutants R66Q, K126Q/K128Q, and F144SF149S, which showed no binding defect to C4b, was at, or just slightly below, wild-type levels in binding to C4dg at either ionic strength. The ΔCCP 4 variant, which displayed wild-type behavior in its C4b binding, displayed ~2-fold diminished binding to the C4dg-coupled chip. For binding to the C4c-coupled chip, the R66Q mutant showed a 2-fold defect in this and other repeat experiments. Similarly, the ~2−3-fold defect seen for the C4c binding activity of the ΔCCP 4 variant was a consistent finding, as was the somewhat enhanced binding of the F144S/F149S variant.

Because of its differential effect on C4c vs C4dg binding, the H67Q C4BP mutant was subjected to a more complete binding analysis in which it was the entity coupled to the biosensor chip, and binding curves were acquired using C4b, C4c, and C4dg as analytes, all at half-physiologic ionic strength. With C4b as the analyte, the extent of the defect in binding observed was much greater when measured under these intrinsic affinity conditions than in the avidity binding situation of the mutant scan series depicted in Figure 8. Specifically, relative to wild-type behavior, C4BP H67Q exhibited an ~6-fold decrease in affinity and an ~13-fold decrease in RU_{max} (Table 1), suggesting that most of the potential binding sites have an affinity that was too low to measure. Even at the highest concentration of C4c employed (1.1 μM), binding to C4BP H67Q was unmeasurable, confirming the large defect seen in the mutant scan experiment. With C4dg as the analyte, however, consistent with the results of the mutant scan series, the effect of the H67Q mutation was quite modest, leading to less than a 2-fold decrease in affinity and a slightly more than 2-fold decrease in RU_{max} (Table 1). The F144S/F149S mutant of C4BP was also analyzed in detail in this experimental format, primarily to ascertain the veracity of the enhanced binding to C4c that was seen in the mutant scan experiment (Figure 8). As can be seen in Table 1, whereas the K_D value for C4c binding is indistinguishable from wild type, the RU_{max} value is about twice that of wild type, suggesting that this mutation actually favors formation of a C4c-capable binding site. However, it does not seem to translate into an effect that is seen when the binding of C4b is analyzed as the latter displays a wild-type-like K_D and its maximal binding to C4BP F144S/F149S (740 RU) is actually somewhat lower than expected for the number of RU units coupled. Binding of C4dg to this mutant is at most marginally less than expected for wild-type behavior (Table 1). Finally, the wild-type-like behavior of the R66Q C4BP mutant seen in the mutant scan experiment (Figure 8) was confirmed in the intrinsic affinity experimental format by the similarity of both the K_D and RU_{max} values for each of C4b, C4c, and C4dg to those determined for their respective binding to wild-type C4BP (Table 1).

Collectively, the data suggest that most of the positively charged residues at the CCP 1−CCP 2 interface that have previously been implicated in mediating binding of C4b are recognizing a negative patch formed by a surface where the C4dg domain abuts the larger C4c fragment. In the structure of C4BP 1−2 (*14*), H67 is somewhat distal to the positive cluster at the interface of CCP 1 and CCP 2, but still within CCP 2, and since this mutation affects C4b and C4c, but

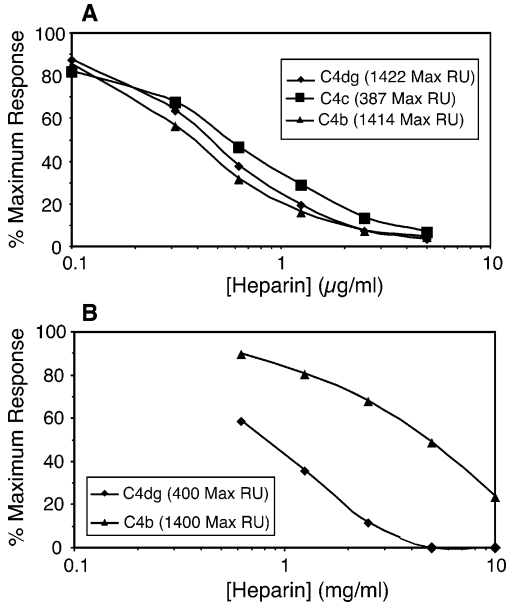

FIGURE 9: Inhibition of wild-type C4BP binding to C4b and its subfragments by heparin. Wild-type C4BP at 10 μg/mL was preincubated with varying concentrations of heparin before being injected over a biosensor chip mounted in a Biacore 3000 and bearing C4b (triangles), C4c (squares), and C4dg (diamonds). Results are expressed as the percentage of the maximal response at the end of the injection phase in the absence of heparin. The experiment was conducted in both half-physiologic ionic strength buffer (panel A) and physiologic ionic strength buffer (panel B). The signal change due to binding to each channel in the absence of heparin is indicated in the insets.

not C4dg binding, it implies a contact point for H67 in C4c away from a C4dg/C4c interface surface. Similarly, the selective enhancement in C4c binding seen for the F144S/F149S variant of C4BP implies contacts in C4c away from the C4dg/C4c interface. The wild-type-like behavior of the R66Q mutant, for not only the parent C4b molecule but also both subfragments, implies that the guanido side chain of this residue is likely pointing away from the binding surface.

Heparin Affects the Binding of both C4c and C4dg to C4BP. Previous results have shown that the interaction sites in C4BP for C4b and for the polyanion heparin are overlapping (*9*, *10*, *39*). Indeed, not only are they competitive ligands but both deletion of CCP 2 and mutation of the positively charged residues modeled to the CCP 1−CCP 2 interface severely compromise the binding of both C4b and heparin (*7*, *9*). In view of the fact that mutation of the basic residues within the CCP 1−CCP 2 interface adversely affected the binding of both C4c and C4dg, one would predict that heparin should also inhibit C4BP's binding to the C4b subfragments. To test the prediction, as well as to determine the concentration dependence of any heparin inhibition of binding observed, wild-type C4BP at a concentration of 10 μg/mL was preincubated with variable concentrations of heparin before injection over channels on a single biosensor chip that had been coupled with C4b, C4c, and C4dg, respectively. The experiments were preformed at both half-physiologic and at physiologic ionic strength, although in the case of the latter, the level of binding of C4BP to the C4c channel, even in the absence of heparin, was too low to provide an adequate experimental window in which to monitor the effect of heparin preincubation. As can be seen in Figure 9A, at half-physiologic ionic strength, preincubation of C4BP with heparin was inhibitory to the binding of C4BP to C4b, C4c, and C4dg. At this ionic strength, the inhibition curves for both the parent molecule and the subfragments were fairly similar, with midpoints in the range of 0.5−0.7 μg/mL of heparin. Figure 9B shows that, at physiologic ionic strength, a heparin concentration of ~0.8 mg/mL is required to inhibit 50% binding to the C4dg channel, whereas for the C4b channel, a 5-fold higher concentration of heparin was required to achieve the same degree of binding inhibition. That a higher concentration of heparin should be required for inhibition of C4BP binding to C4b is consistent with the stronger affinity of C4BP for C4b than for C4dg. However, the more striking observation is the 3 orders of magnitude difference in the concentration ranges of heparin required to inhibit the protein−protein interactions at physiologic vs half-physiologic ionic strength. This clearly demonstrates that the ionic strength dependence of the C4BP−heparin interaction is much greater than that for the interaction of C4BP with either C4b or C4dg. This is in turn consistent with ionic forces being the dominant contributor to the free energy of binding of the sulfated oligosaccharide heparin to C4BP, whereas for C4BP's binding to protein ligands, ionic forces, while clearly being very important, are one among several forces that contribute to the binding energy.

CONCLUSIONS

The main finding of our study is that not only do the C4c and C4dg subfragments of C4b each contribute sufficiently to the overall binding of the parent molecule to C4BP to be individually measurable but there is a synergistic effect on binding when the subfragments are present together. Mechanistically, the effect of C4c on C4dg binding appears to be through an increase in the binding affinity of C4dg for its binding site in C4BP (Figures 6E,F and 7C,D, Table 2). Since we have observed a weak direct interaction between C4c and C4dg (Figure 4A), part of the increase in C4dg's apparent binding affinity to a subunit simultaneously occupied by C4c could be due to the availability of the C4c contact surface. However, this cannot be the explanation for the effect of C4dg on C4c's binding behavior, where the affinity of binding remains essentially unchanged, but based on the change in apparent RU_{max}, there is an ~3-fold increase in apparent site number (Table 2). Since in our treatment of the data we had already corrected for any RU change due to independent C4dg binding to C4BP, if the increase in RU_{max} from the analysis of binding curves, such as the ones in Figures 6C and 7A, was solely due to C4dg binding directly to every C4c molecule that was bound to C4BP in the absence of C4dg, the fold increase in RU_{max} should simply reflect the ratio of the sum of the molecular masses of C4c plus C4dg, divided by that of C4c alone, specifically ~1.3-fold. Since the RU_{max} increase was substantially greater than 1.3-fold, it becomes necessary to interpret this change as reflecting binding of C4c to sites, which in the absence of C4dg binding, would remain unoccupied. The simplest explanation is that there exists an equilibrium between a high-affinity C4c-binding conformation and a much lower affinity conformation. Indeed, we have consistently observed that the greatest deviation from single class binding site behavior for immobilized C4BP occurred when C4c was the analyte. We propose that C4dg binding shifts the conformational equilibrium to the one having a higher affinity for C4c. A

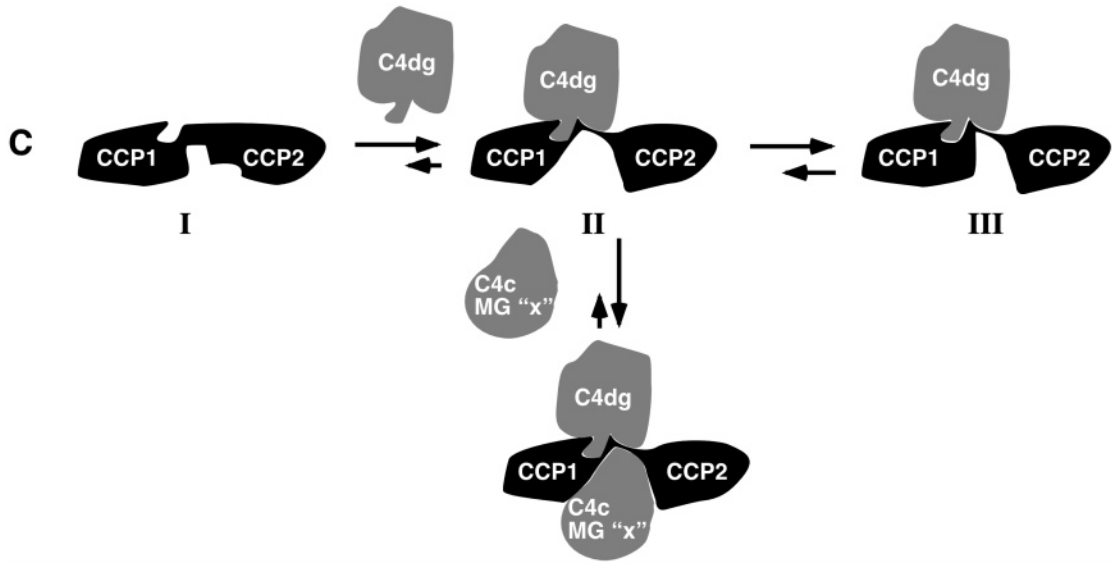

FIGURE 10: Model for the synergies observed in C4BP subsite binding. Panel A: Within the context of the C4b molecule, the thioester domain/C4d portion of C4dg has a domain interface with a yet to be identified C4c subdomain [denoted MG"x", as per the C3 structure nomenclature (*47*)] that mediates a major contact to C4BP. Panel B: The primary binding site in C4BP is comprised of residues at the interface of CCP 1 and CCP 2. Within a C4BP subunit, these domains are depicted as existing as an equilibrium mixture of two conformational states (**I** and **II**) that differ predominantly in their intermodular orientations and, thus, in the alignment of residues at the interface between the domains. In the absence of ligand, the equilibrium strongly favors conformation **I** (note relative size of arrows), but only conformation **II** has a fully formed C4c binding subsite. Panel C: For the case corresponding to experiments in which C4dg and C4c were present at the same time, but as separate molecular entities, the first encounter is with C4dg, which either stabilizes conformation **II** or, if it binds to conformation **I**, induces through some additional contacts formed a shift in the equilibrium to conformation **II**. C4c can now bind to a greater number of sites than would have been present in the absence of C4dg. The reestablishment of the relatively small domain interface between C4dg and C4c would enhance the affinity of the binding interaction of C4dg to C4BP; however, given the much larger buried surface area depicted for the contact with C4c, this additional domain interface contact with C4dg has a negligible effect on the overall affinity governing C4c binding. If C4c is not immediately available to bind to the C4dg-liganded conformation **II**, conformational species **III** may form, which is refractory to C4c binding. This species is invoked to explain the observation in Figure 5 that prebinding of C4dg to C4BP renders the latter refractory to binding to a C4c-coupled biosensor chip. However, in the physiologically relevant situation, i.e., the ligand is C4b, the relevant contacting surfaces in C4dg and C4c for C4BP would be present within the same molecular entity. Assuming the same general mechanism for ordered subsite filling in which the initial encounter complex was with the C4dg moiety, the C4c subsite would be immediately filled and little, if any, of conformational species **III** would form.

cartoon depiction of our model to explain the synergistic binding behavior of the C4b subfragments to subsites in a C4BP monomeric subunit is presented in Figure 10. It is elaborated upon further below, as well as in the figure legend.

As recently reviewed (*40*), there are numerous examples in the structural literature where there are significant conformational differences between unliganded and liganded proteins. Although many of these cases are ascribed to "induced fit"-type conformational changes in a binding site after an initial contact with the ligand, a subset of the cases conform with there being a "preequilibrium" in which the protein exists in two distinct conformational states, only one of which is capable of binding a particular ligand and is therefore the only one seen in a cocrystal of the protein and ligand. A case in point is the IgE monoclonal antibody Spe7 whose combining site has been visualized in two very different conformations (*41*), flat and funnel-shaped, determined mainly by the conformational isomerization of the V_H CDR3 and V_LCDR3 loops of the combining site. The conformation having the relatively flat combining site is the only one seen in complex with a macromolecular protein antigen. By contrast, the conformation with a funnel-shaped combining site is the only one seen in complex with a small hapten. It is inferred that the preexisting equilibrium is shifted from one combining site conformer to the other by complex formation with the appropriate ligand. Returning to the case of the C4BP binding site for C4b, while it is clear from the relative affinities of C4c and C4dg that the major binding energy comes from contacts with the C4c portion of the molecule (represented by its large contact surface in the cartoon model, Figure 10C), prior, or at least simultaneous, encounter with C4dg induces, or stabilizes, the adjacent C4c subsite in the binding-competent conformation and therefore increases its equilibrium concentration (Figure 10C). This in turn suggests that the contact regions within C4BP should be deformable and may explain how divergent ligands such as C4b, heparin (*7*, *42*), DNA (*13*), and microbial binding partners of C4BP such as the M-proteins of group A *Streptococcus* (*12*) or the filamentous hemagglutinin from *Bordetella pertusus* (*43*) can bind to overlapping, although not identical binding sites in C4BP.

The identification of residues comprising the CCP 1−CCP 2 interface as contributing to both the C4c and C4dg subsites (Figure 8B,C) suggests that the conformational change should be in this area. A number of structural studies on CCP-containing proteins have shown that the segments joining adjacent CCP domains are quite flexible and that this in turn results in an ensemble of interdomain tilt and twist angles being adopted (*44*, *45*). Additionally, a recent NMR study that examined the backbone dynamics of CCP 16 of CR1, which is the middle domain of the C3b binding site, found that the segments identified through site-directed mutagenesis as contributing to the binding of C3b were also among the most mobile in the domain and, conversely, that a face of the domain known not to be involved in C3b binding was quite rigid (*46*). The same study found that with the first

CCP domain of MCP, there was also a correlation between conformational flexibility observed and segments identified through mutagenesis as contributing to the binding of either C4b or measles virus hemagglutinin protein to MCP. Finally, the very recently obtained structure of CCP 1−2 of the C4BP α-chain provides compelling evidence for conformational flexibility being a component of ligand binding by C4BP (*14*). First, the structure shows that in order for all of the residues implicated by mutageneisis as being essential for C4b binding to be brought into juxtaposition, a twist between the modules is required. Second, the binding to CCP 1−2 of a 45-residue dimeric peptide from the NH_2 terminus of streptococcal M-protein, a ligand whose binding site partially overlaps that of C4b, induces large chemical shift changes in several peaks of the $^{1}H-^{15}N$ HSQC spectrum that arise from residues localized to the intermodular area. The authors argue that ligand-induced intermodular conformational movements most readily explain the observed spectral changes.

To date, the C4d fragment is the only part of C4 for which there is a high-resolution structure (*37*). Very recently, however, an X-ray crystal structure for the entire C3 molecule has been published (*47*), and it is reasonable to surmise, based on pairwise sequence identities in the 27−30% range, that C3, C4, and C5 will have similar overall domain architectures. A space-filling model of the native C3 molecule shows that there is quite a large area where the C3d domain interacts with several of the constituent domains of C3c and one assumes that the same would hold true for the apposition of C4d and C4c. The involvement of the basic residues at the CCP 1−2 interface of C4BP in the interaction with both the C4dg and C4c subfragments, as indicated by the compromised interactions of the isolated subfragments with several C4BP mutants having a decreased net positive charge in this area, suggests that somewhere along the interface between C4c and C4d there should be a surface of significant negative charge that interacts with the identified basic residues in CCP 1 and CCP 2. However, as discussed by Jannsen et al. (*47*) in the context of the native C3 structure and its comparison to that of C3c, several domains of the α-chain undergo major orientation changes, some of which must occur at the C3b stage. Although lack of knowledge on the orientation of α-chain domains at the C3b stage precludes the usefulness of sequence alignment-based homology modeling of C4 to identify the C4c domains involved in binding C4BP by simply looking for a negatively charged patch that forms a continuous surface with C4d, the knowledge of the domain boundaries from the C3 structure should enable candidate C4c domains such as MG2, MG6, MG7, or MG8 to be expressed and individually tested for their potential interaction with wild-type and mutant forms of C4BP.

ACKNOWLEDGMENT

We are grateful to Drs. Daniel J. Dumont and Eric Yang of the Centre for Proteomic and Genomic Studies, Sunnybrook and Women's College Health Sciences Centre, Toronto, for the generous access to their Biacore 3000 instrument. Similarly, we thank Dr. John Glover of the Department of Biochemistry, University of Toronto, for generous access to his Biacore-X instrument.

REFERENCES

1. Kirkitadze, M. D., and Barlow, P. N. (2001) Structure and flexibility of the multiple domain proteins that regulate complement activation, *Immunol. Rev. 180*, 146−161.
2. Seet, B. T., Johnston, J. B., Brunetti, C. R., Barrett, J. W., Everett, H., Cameron, C., Sypula, J., Nazarian, S. H., Lucas, A., and McFadden, G. (2003) Poxviruses and immune evasion, *Annu. Rev. Immunol. 21*, 377−423.
3. Mullick, J., Bernet, J., Singh, A. K., Lambris, J. D., and Sahu, A. (2003) Kaposi's sarcoma-associated herpesvirus (human herpesvirus 8) open reading frame 4 protein (kaposica) is a functional homolog of complement control proteins, *J. Virol. 77*, 3878−3881.
4. Spiller, O. B., Blackbourn, D. J., Mark, L., Proctor, D. G., and Blom, A. M. (2003) Functional activity of the complement regulator encoded by Kaposi's sarcoma-associated herpesvirus, *J. Biol. Chem. 278*, 9283−9289.
5. Spiller, O. B., Robinson, M., O'Donnell, E., Milligan, S., Morgan, B. P., Davison, A. J., and Blackbourn, D. J. (2003) Complement regulation by Kaposi's sarcoma-associated herpesvirus ORF4 protein, *J. Virol. 77*, 592−599.
6. Blom, A. M., Villoutreix, B. O., and Dahlback, B. (2004) Complement inhibitor C4b-binding protein-friend or foe in the innate immune system?, *Mol. Immunol. 40*, 1333−1346.
7. Blom, A. M., Kask, L., and Dahlback, B. (2001) Structural requirements for the complement regulatory activities of C4BP, *J. Biol. Chem. 276*, 27136−27144.
8. Ziccardi, R. J., Dahlback, B., and Muller-Eberhard, H. J. (1984) Characterization of the interaction of human C4b-binding protein with physiological ligands, *J. Biol. Chem. 259*, 13674−13679.
9. Blom, A. M., Webb, J., Villoutreix, B. O., and Dahlback, B. (1999) A cluster of positively charged amino acids in the C4BP alpha-chain is crucial for C4b binding and factor I cofactor function, *J. Biol. Chem. 274*, 19237−19245.
10. Villoutreix, B. O., Hardig, Y., Wallqvist, A., Covell, D. G., Garcia de Frutos, P., and Dahlback, B. (1998) Structural investigation of C4b-binding protein by molecular modeling: localization of putative binding sites, *Proteins 31*, 391−405.
11. Blom, A. M., Zadura, A. F., Villoutreix, B. O., and Dahlback, B. (2000) Positively charged amino acids at the interface between alpha-chain CCP1 and CCP2 of C4BP are required for regulation of the classical C3-convertase, *Mol. Immunol. 37*, 445−453.
12. Blom, A. M., Berggard, K., Webb, J. H., Lindahl, G., Villoutreix, B. O., and Dahlback, B. (2000) Human C4b-binding protein has overlapping, but not identical, binding sites for C4b and streptococcal M proteins, *J. Immunol. 164*, 5328−5336.
13. Trouw, L. A., Nilsson, S. C., Goncalves, I., Landberg, G., and Blom, A. M. (2005) C4b-binding protein binds to necrotic cells and DNA, limiting DNA release and inhibiting complement activation, *J. Exp. Med. 201*, 1937−1948.
14. Jenkins, H. T., Mark, L., Ball, G., Persson, J., Lindahl, G., Uhrin, D., Blom, A. M., and Barlow, P. N. (2006) Human C4b-binding protein−structural basis for interaction with streptococcal M protein, a major bacterial virulence factor, *J. Biol. Chem. 281*, 3690−3697.
15. Becherer, J. D., and Lambris, J. D. (1988) Identification of the C3b receptor-binding domain in third component of complement, *J. Biol. Chem. 263*, 14586−14591.
16. Jokiranta, T. S., Westin, J., Nilsson, U. R., Nilsson, B., Hellwage, J., Lofas, S., Gordon, D. L., Ekdahl, K. N., and Meri, S. (2001) Complement C3b interactions studied with surface plasmon resonance technique, *Int. Immunopharmacol. 1*, 495−506.
17. Clemenza, L., and Isenman, D. E. (2004) The C4A and C4B isotypic forms of human complement fragment C4b have the same intrinsic affinity for complement receptor 1 (CR1/CD35), *J. Immunol. 172*, 1670−1680.
18. Sharma, A. K., and Pangburn, M. K. (1996) Identification of three physically and functionally distinct binding sites for C3b in human complement factor H by deletion mutagenesis, *Proc. Natl. Acad. Sci. U.S.A. 93*, 10996−11001.
19. Jokiranta, T. S., Hellwage, J., Koistinen, V., Zipfel, P. F., and Meri, S. (2000) Each of the three binding sites on complement factor H interacts with a distinct site on C3b, *J. Biol. Chem. 275*, 27657−27662.
20. Kuhn, S., Skerka, C., and Zipfel, P. F. (1995) Mapping of the complement regulatory domains in the human factor H-like protein 1 and in factor H1, *J. Immunol. 155*, 5663−5670.

21. Gordon, D. L., Kaufman, R. M., Blackmore, T. K., Kwong, J., and Lublin, D. M. (1995) Identification of complement regulatory domains in human factor H, *J. Immunol. 155*, 348−356.
22. Alsenz, J., Lambris, J. D., Schulz, T. F., and Dierich, M. P. (1984) Localization of the complement-component-C3b-binding site and the cofactor activity for factor I in the 38kDa tryptic fragment of factor H, *Biochem. J. 224*, 389−398.
23. Pangburn, M. K. (2002) Cutting edge: localization of the host recognition functions of complement factor H at the carboxyl-terminal: implications for hemolytic uremic syndrome, *J. Immunol. 169*, 4702−4706.
24. Guthridge, J. M., Rakstang, J. K., Young, K. A., Hinshelwood, J., Aslam, M., Robertson, A., Gipson, M. G., Sarrias, M. R., Moore, W. T., Meagher, M., Karp, D., Lambris, J. D., Perkins, S. J., and Holers, V. M. (2001) Structural studies in solution of the recombinant N-terminal pair of short consensus/complement repeat domains of complement receptor type 2 (CR2/CD21) and interactions with its ligand C3dg, *Biochemistry 40*, 5931−5941.
25. Diefenbach, R. J., and Isenman, D. E. (1995) Mutation of residues in the C3dg region of human complement component C3 corresponding to a proposed binding site for complement receptor type 2 (CR2, CD21) does not abolish binding of iC3b or C3dg to CR2, *J. Immunol. 154*, 2303−2320.
26. Clemenza, L., and Isenman, D. E. (2000) Structure-guided identification of C3d residues essential for its binding to complement receptor 2 (CD21), *J. Immunol. 165*, 3839−3848.
27. Kalli, K. R., Ahearn, J. M., and Fearon, D. T. (1991) Interaction of iC3b with recombinant isotypic and chimeric forms of CR2, *J. Immunol. 147*, 590−594.
28. Esparza, I., Becherer, J. D., Alsenz, J., De la Hera, A., Lao, Z., Tsoukas, C. D., and Lambris, J. D. (1991) Evidence for multiple sites of interaction in C3 for complement receptor type 2 (C3d/EBV receptor, CD21), *Eur. J. Immunol. 21*, 2829−2838.
29. Sarrias, M. R., Franchini, S., Canziani, G., Argyropoulos, E., Moore, W. T., Sahu, A., and Lambris, J. D. (2001) Kinetic analysis of the interactions of complement receptor 2 (CR2, CD21) with its ligands C3d, iC3b, and the EBV glycoprotein gp350/220, *J. Immunol. 167*, 1490−1499.
30. Bernet, J., Mullick, J., Panse, Y., Parab, P. B., and Sahu, A. (2004) Kinetic analysis of the interactions between vaccinia virus complement control protein and human complement proteins C3b and C4b, *J. Virol. 78*, 9446−9457.
31. Blom, A. M., Villoutreix, B. O., and Dahlback, B. (2003) Mutations in alpha-chain of C4BP that selectively affect its factor I cofactor function, *J. Biol. Chem. 278*, 43437−43442.
32. Dodds, A. W. (1993) Small-scale preparation of complement components C3 and C4, *Methods Enzymol. 223*, 46−61.
33. Hessing, M., Paardekooper, J., and Hack, C. E. (1993) Separation of different forms of the fourth component of human complement by fast protein liquid chromatography, *J. Immunol. Methods 157*, 39−48.
34. Nagasawa, S., Ichihara, C., and Stroud, R. M. (1980) Cleavage of C4b by C3b inactivator: production of a nicked form of C4b, C4b′, as an intermediate cleavage product of C4b by C3b inactivator, *J. Immunol. 125*, 578−582.
35. Nagasawa, S., and Stroud, R. M. (1980) Purification and characterization of a macromolecular weight cofactor for C3b-inactivator, C4bC3bINA-cofactor, of human plasma, *Mol. Immunol. 17*, 1365−1372.
36. Hammer, C. H., Wirtz, G. H., Renfer, L., Gresham, H. D., and Tack, B. F. (1981) Large scale isolation of functionally active components of the human complement system, *J. Biol. Chem. 256*, 3995−4006.
37. van den Elsen, J. M., Martin, A., Wong, V., Clemenza, L., Rose, D. R., and Isenman, D. E. (2002) X-ray crystal structure of the C4d fragment of human complement component C4, *J. Mol. Biol. 322*, 1103−1115.
38. Nagar, B., Jones, R. G., Diefenbach, R. J., Isenman, D. E., and Rini, J. M. (1998) X-ray crystal structure of C3d: a C3 fragment and ligand for complement receptor 2, *Science 280*, 1277−1281.
39. Hessing, M., Vlooswijk, R. A., Hackeng, T. M., Kanters, D., and Bouma, B. N. (1990) The localization of heparin-binding fragments on human C4b-binding protein, *J. Immunol. 144*, 204−208.
40. Goh, C. S., Milburn, D., and Gerstein, M. (2004) Conformational changes associated with protein−protein interactions, *Curr. Opin. Struct. Biol. 14*, 104−109.
41. James, L. C., Roversi, P., and Tawfik, D. S. (2003) Antibody multispecificity mediated by conformational diversity, *Science 299*, 1362−1367.
42. Villoutreix, B. O., Blom, A. M., Webb, J., and Dahlback, B. (1999) The complement regulator C4b-binding protein analyzed by molecular modeling, bioinformatics and computer-aided experimental design, *Immunopharmacology 42*, 121−134.
43. Berggard, K., Lindahl, G., Dahlback, B., and Blom, A. M. (2001) *Bordetella pertussis* binds to human C4b-binding protein (C4BP) at a site similar to that used by the natural ligand C4b, *Eur. J. Immunol. 31*, 2771−2780.
44. Stehle, T., and Larvie, M. (2003) Structures of complement control proteins, in *Infectious Disease: Innate Immunity* (Rab, E., and Ja, H., Eds.) pp 231−253, Humana Press, Totowa, NJ.
45. Smith, B. O., Mallin, R. L., Krych-Goldberg, M., Wang, X., Hauhart, R. E., Bromek, K., Uhrin, D., Atkinson, J. P., and Barlow, P. N. (2002) Structure of the C3b binding site of CR1 (CD35), the immune adherence receptor, *Cell 108*, 769−780.
46. O'Leary, J. M., Bromek, K., Black, G. M., Uhrinova, S., Schmitz, C., Wang, X., Krych, M., Atkinson, J. P., Uhrin, D., and Barlow, P. N. (2004) Backbone dynamics of complement control protein (CCP) modules reveals mobility in binding surfaces, *Protein Sci. 13*, 1238−1250.
47. Janssen, B. J., Huizinga, E. G., Raaijmakers, H. C., Roos, A., Daha, M. R., Nilsson-Ekdahl, K., Nilsson, B., and Gros, P. (2005) Structures of complement component C3 provide insights into the function and evolution of immunity, *Nature 437*, 505−511.

BI0603827